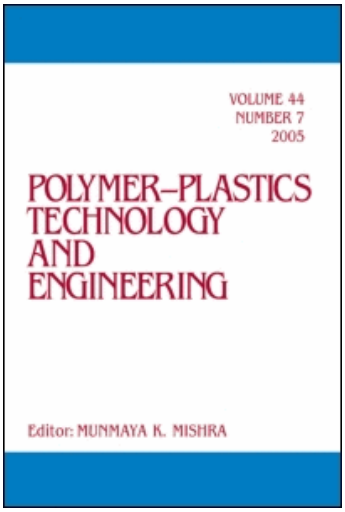

Polymer-Plastics Technology and Engineering
Publication details, including instructions for authors and subscription information:
http://www.informaworld.com/smpp/title~content=t713925971

Biodegradable Bovine Gelatin/Na⁺-Montmorillonite Nanocomposite Films. Structure, Barrier and Dynamic Mechanical Properties

J. F. Martucci [a];R. A. Ruseckaite [a]
[a] Research Institute of Material Science and Technology (INTEMA), J. B. Justo, Mar del Plata, Argentina

Online publication date: 03 May 2010

To cite this Article Martucci, J. F. andRuseckaite, R. A.(2010) 'Biodegradable Bovine Gelatin/Na⁺-Montmorillonite Nanocomposite Films. Structure, Barrier and Dynamic Mechanical Properties', Polymer-Plastics Technology and Engineering, 49: 6, 581 — 588
To link to this Article: DOI: 10.1080/03602551003652730
URL: http://dx.doi.org/10.1080/03602551003652730

Polymer-Plastics Technology and Engineering, 49: 581–588, 2010

ISSN: 0360-2559 print/1525-6111 online
DOI: 10.1080/03602551003652730

Taylor & Francis
Taylor & Francis Group

Biodegradable Bovine Gelatin/Na^+-Montmorillonite Nanocomposite Films. Structure, Barrier and Dynamic Mechanical Properties

J. F. Martucci and R. A. Ruseckaite
Research Institute of Material Science and Technology (INTEMA), J. B. Justo, Mar del Plata, Argentina

Biodegradable films based on gelatin and Na^+-Montmorillonite were prepared by mixing of gelatin solutions with ultrasonically pre-treated clay suspensions under controlled conditions. The DRX patterns and AFM images suggested that ultrasonication process resulted in homogeneously distributed layered silicates inside the matrix but not fully exfoliated. Transparency was retained, suggesting that filler is mostly distributed at the nanoscale. The results of DMA showed an improvement in storage modulus and shifts in tan δ peaks toward higher temperatures. The reduction in polar groups due to hydrogen interactions between gelatin and clay particles was evidenced by the decrease in surface hydrophilicity and WVP.

Keywords Bio-nanocomposite; Dynamic mechanical properties; Gelatin; Montmorillonite; Physical properties

INTRODUCTION

Gelatin (Ge) is a mixture of high molar-mass polypeptides produced from collagenous animal tissue. It can be visualized as a copolymer build up from triads of α-aminoacids with glycine (Gly) at every third position (soft blocks) and triads of hydroxyproline (Hypro), proline (Pro) and glycine (rigid blocks), with a narrow molar mass distribution[1]. Due to its high gas barrier properties, film-forming ability, low cost and biodegradability gelatin is an interesting alternative to synthetic plastics mainly in those applications where biodegradability gives an added value (i.e., packaging)[2,3]. The use of gelatin-based materials has been restricted because of their inherent water sensitivity and relatively low stiffness and strength, especially in moist environments. Therefore, gelatin-based materials must be modified to be competitive to petroleum-based polymers in question of performance[4]. One way to overcome these limitations and greatly enhance the commercial potential of gelatin-based materials is to incorporate nanosized reinforcements[5,6], such as layered silicates to produce environmentally friendly nanocomposites.

Address correspondence to J. F. Martucci, Research Institute of Material Science and Technology (INTEMA), J. B. Justo 4302, Mar del Plata 7600, Argentina. E-mail: jmartucci@fi.mdp.edu.ar

Nanocomposites based on biopolymers, also called bio-nanocomposites with improved stiffness, strength, toughness, thermal stability, barrier properties and flame retardancy have been documented[7–16], and some of them could be considered as potential alternatives to petroleum-based polymers, particularly at the packaging sector[17]. Nano-reinforcements are also unique in that they will not affect the clarity of the polymer matrix[18]. Moreover, biodegradability is retained; that is, after final degradation, only inorganic, natural minerals (clay) will be left[19,20].

Our current work is focused on preparing Ge-Na^+-Montmorillonite nanocomposite films intended to be used as component of biodegradable multilayer films based on gelatin with potential application at the packaging sector[15,20]. The aim of the present study was to evaluate the performance of nanocomposites films with different clay content in terms of their transparency, dynamic mechanical properties, surface hydrophobicity, moisture resistance and water vapor permeability. Interactions between matrix and filler were also analyzed and related to the functional properties of the films.

EXPERIMENTAL AND MATERIAL METHODS

Materials

Bovine gelatin (Ge) type B was kindly supplied by Rousselot (Argentina), Bloom 150, isoionic point (Ip_{Ge}) 5.3. Sodium montmorillonite nanoclay (MMt) was purchased from Southern Clay Products Inc. (Texas, USA), under the trade name Cloisite Na^+. The cation-exchange capacity (CEC) was 92.6 meq/100 mg clay, and the interlayer distance was 1.2 nm (as it was determined by X-ray diffraction on the dried powder)[21].

Bio-Nanocomposite Films Preparation

Due to its polyelectrolyte character gelatin can easily insert between philosilicate layers in montmorillonite (MMt) to produce intercalated or exfoliated nanocomposites, without using liophilization. Therefore, gelatin-based

nanocomposites were prepared by the solution intercalation method[5,7,22] and following the same technique described elsewhere[15].

Basically, a desired amount of gelatin powder was hydrated in distilled water at 50°C and the pH was adjusted to 7 (higher than $Ip_{Ge} = 5.3$) with NaOH 0.1N. In parallel, a desired amount of MMt (final content between 0 to 17 wt.% on dry matter basis) was swollen in distilled water and treated ultrasonically at 50°C during 20 min.

Subsequently, the aqueous gelatin solution was added drop-wise into clay suspension and mixed together at 50°C under vigorous stirring during 15 min. The resultant aqueous suspensions were then cast in Teflon molds (10 mm diameter) and dried at 50°C during 15 h in a convection oven. The obtained materials were labelled as **Ge/XMMt**, where **X** corresponds to the weight percentage of montmorillonite. Similar processing conditions as those described for the composites were used to process MMt-free gelatin films. The average thickness of the dry films was about $200 \pm 50\,\mu m$.

X-Ray Diffraction

X-ray Diffraction patterns were recorded using a Phillips PW1700 diffractometer equipped with Cu Kα radiation source ($\lambda = 0.1546$ nm), operating at 45 KV and 30 mA as the applied voltage and current, respectively. The incidence angle was varied between 2 and 12° at a scanning rate of 1°/min.

Atomic Force Microcopy (AFM)

AFM measurements were carried out in hard tapping mode (HT-AFM) using a Nanoscope IIIa Multimode apparatus from Digital Instruments. Before testing, the microscope was allowed to equilibrate at 25°C and kept at this temperature during all the experiments. Images were recorded using an integrated silicon tip/cantilever (Digital Inst.) having a resonance frequency of 1 Hz. The specimens were cross-sectioned under liquid nitrogen for obtaining smooth surfaces. All the images are shown without any further image processing treatment.

Fourier Transformed Infrared Spectrometry (FTIR)

Interactions in Ge/MMt nanocomposites were investigated by Fourier Transform Infrared Spectroscopy (FTIR) analysis by using a Mattson Genesis II spectrophotometer in transmission mode. The measurements were recorded between 4000–400 cm^{-1} at 32 scans. Pulverized specimens were pressed into pellets with KBr. The background noise was corrected with pure KBr data.

Opacity

Film opacity was determined according to the method described by Irissin-Mangata et al.[23] on rectangular strips placed in a UV-Visible spectrophotometer test cell directly. The absorption spectrum of the sample was obtained from 400 to 800 nm in a UV-Visible spectrophotometer Shimadzu 1601 PC. Film opacity was defined as the area under the recorded curve which was obtained through an integration procedure and it was expressed as Absorbance units (nm) per thickness unit (μm).

Contact Angle Measurements

Surface hydrophobicity was evaluated by static contact angle measurements using a home-made instrument which allowed the determination of contact angle at equilibrium, with a precision of ±1° at 25°C. A drop (≈0.5 μL) of diiodomethane or ethylenglycol (Aldrich Co.) was deposited onto the film surface with an automatic piston syringe and photographed using a digital camera after stabilization (about 5 min). An image analyser was used to measure the angle formed between the base, constituted of the surface of the film in contact with the drop, and the tangent to the drop of liquid. From the static data with pure liquids of different polarity, the dispersive (γ_s^d) and polar (γ_s^p) components contributions to the surface free energy (γ) were obtained by using the geometric approach[24]. Results were the mean values of six independent measurements.

Water Uptake at 65% Relative Humidity (RH)

Water uptake tests were performed gravimetrically. Samples were dried until constant weight in an oven to remove the moisture before testing and this weight was taken as the initial one (m_0). After this, samples were conditioned at 25° in humidity chamber at $65 \pm 2\%$ RH. Samples were removed at specifics intervals (t) and the increment in weight of the specimens (m_t) was measured. The moisture content (w_t) as a function of time t was obtained from the total and partial (water) mass balance over the sample as a function of time:

$$WU(\%) = \frac{m_0 * w_0 + (m_t - m_0) * 100\%}{m_t} \qquad (1)$$

where w_t is the moisture content as a function of time (%), m_t is the weight of the sample after exposition, m_0 is the initial weight and w_0 is the initial moisture content of the samples.

To determine the water absorption rate, the apparent diffusion coefficient (D_{app} m^2/seg) was calculated from the following relationship[25,26].

$$\frac{m_t - m_0}{m_\infty - m_0} = 1 - \sum_{n=0}^{\infty} \frac{8}{(2n+1)^2 * \pi^2} \times \exp\left(\frac{-D_{app} * (2n+1)^2 * \pi^2 * t}{e^2}\right) \qquad (2)$$

where e is the film thickness (m), m_∞ is the weight of the sample in the equilibrium (g). Composite materials do not fulfil the requirements of a simple Fick's law. Equation (2) takes into account that diffusion in composite materials is affected by different factors such as (a) the inhomogeneous nature of composite materials, (b) the presence of interactions between filler and matrix, (c) water may diffusion through filler-matrix interphace, (d) some extractable can be removed during water absorption and (e) dimensions of the specimens may change during the experiment[27].

Barrier Properties

Water vapor permeability (WVP $\mathrm{Kg \cdot m/Pa \cdot s \cdot m^2}$) was calculated as:

$$WVP = \frac{(WVT * e)}{\Delta P} \tag{3}$$

where WVT ($\mathrm{Kg/s \cdot m^2}$) is the vapor transmission rate through a mean film thickness e (m) and ΔP is the actual difference in partial water vapor pressure between the two sides of film specimens (Pa). WVP was determined gravimetrically according to ASTM E96-95 dissecant method. Test cells were placed in an environmental chamber at 25°C and $65 \pm 2\%$ RH. The weight change (± 0.0001 g) of the cups versus time was recorded at specific intervals (t) and then plotted. Linear regression was used to calculate the slope of a fitted straight line, which represented the WVT, as follows:

$$WVT = \frac{\Delta m}{t * A} \tag{4}$$

where Δm is the mass change of the cell test (Kg), t is the time (s) and A is the test area ($\mathrm{m^2}$). Permeability was calculated according to:

$$WVP\ (\mathrm{Kg \cdot m/m^2 \cdot s \cdot Pa}) = \frac{WVT}{S * (HR_1 - HR_2)} * e \tag{5}$$

where e is the film thickness (m), S is the saturation pressure (Pa) at the test temperature, $HR1$ is the relative humidity in the test chamber and $HR2$ is the relative humidity inside the cell test. All measurements were performed by quintuplicate.

Dynamic Mechanical Analysis (DMA)

Dynamic Mechanical Analysis (DMA) was performed in a Perkin Elmer dynamic mechanical analyzer (DMA 7-e) in dynamic mode. Tests were performed in tensile mode. Results were the average of three replicates.

RESULTS AND DISCUSSION

Figure 1a shows the XRD patterns of the as – received Cloisite Na^+ and unfilled gelatin (control) film. The free-MMt gelatin film exhibited a broad and low intensity peak in the range of 6.2° to 9.5° characteristic of amorphous proteins[28]. Cloisite Na^+ showed a single peak at $2\theta = 7.3°$ corresponding to a d-spacing (001) of silicate layer of 1.2 nm, according to the Bragg equation. This peak was in the same range of that of amorphous gelatin, therefore in order to visualise any change due to nanocomposite formation, Ge/MMt curves were normalized against a gelatin one, and results are represented in Figure 1b. It is worthy to note that there was no diffraction peak corresponding to MMt basal spacing at least for clay loadings up to 17 wt.%.

The appearance of new peaks shifted toward lower angles indicated a high degree of the nanoclay dispersion[5,6]. The broadening of these peaks indicated that

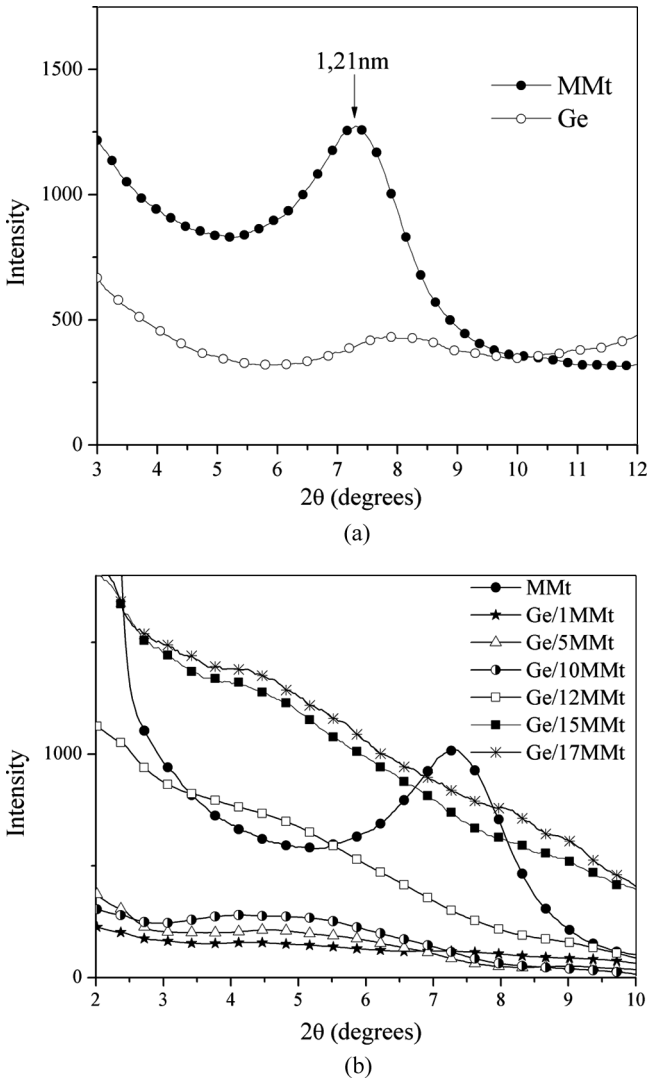

FIG. 1. (a) X-ray diffractograms of untreated Na^+-montmorillonite and neat gelatin film; (b) normalized XRD diffractograms of composites with clay content varying from 1 to 17 wt.% clay.

distances between layers were widen, suggesting that intercalated (or disordered intercalated) nanocomposites were obtained, even at high clay loadings[29]. This result allowed presuming that some kind of strong interactions between gelatin and MMt were established and contributed to maintain a stable nanoclay distribution within the matrix. Interactions between matrix and clay were already reported for various biopolymer/layered silicate systems[8,10,11,30]. In particular, hydrogen interactions between carboxylate from gelatin and hydroxyl groups from MMt at $pH > Ip_{Ge}$ were quite recently proposed[22], based on simulation with low molecular weight molecules. However, and to the best of our knowledge, there is little information about the understanding of the interactions directly performed on Ge/MMt nanocomposites.

To analyze such interactions, FTIR spectra for pure gelatin and bio-nanocomposites with different clay contents were studied and compared. Figure 2 represents the FTIR spectrum of Ge/MMt at 1800–1100 cm^{-1} (amide region). The strong bands in free-MMt gelatin films and composites at 1656 and 1541 cm^{-1} were assigned to the amide I (C=O stretching) and amide II (N−H bending and C−N stretching modes). Amide III (around 1200 cm^{-1}) band was rather complex, consisting of components from C−N stretching and N−H in plane bending from amide linkages, as well as absorptions arising from wagging vibrations from CH_2 groups from the glycine backbone and proline side-chains[31].

In composites, the amide I and II bands became multiple with the presence of clay. This indicated the occurrence of hydrogen bonding interactions between hydrogen atom in gelatin peptide bonds and acceptor atoms such as oxygen from free-OH and Si–O–Si groups in MMt. Similar results were observed for soy protein isolate/montmorillonite systems[11]. It is interesting to note that multiplicity decreased as clay loading increased. This implied that hydrogen interactions became weaker as the average distance between silicates particles decreased. Therefore, some degree of accumulation would be expected at high clay contents.

AFM was used to directly investigate Ge/MMt morphology[32,33]. Usually, transmission electronic microscopy (TEM)[5,6] is used to characterize nanocomposite morphologies. However, this technique fails because cryo-ultramicrotoming procedure damaged the Ge/MMt specimens. Figure 3 shows representative HT-AFM phase images of the obtained films. The surface of free-MMt gelatin film (Figure 3a) was smooth with some irregularities that might be originated during the casting process. The AFM surface of the Ge/10MMt film showed the presence of silicate particles distributed uniformly in the matrix which were visible as light streaks (Figure 3b). The observed AFM structures were consistent with XRD measurements.

Film opacity provided additional information about the particle size of the dispersed phase in the gelatin matrix. For high translucency, the dispersed phase should have an average size smaller than the wavelength of visible light (400–800 nm)[14,23]. However, opacity may be affected by various factors including film thickness. In this study, there was no significant difference in the average thickness, being 195 ± 14 μm for free-MMt gelatin film and 220 ± 35 μm for Ge/10MMt. As can be concluded from Figure 4, gelatin control film exhibited the lower opacity due to the absence of light blockage particles.

As clay content increased, the films showed higher opacity, reflecting that there was strong scattering of MMT resulting in lower transparency of the UV-visible light[14]. Insets in Figure 4 showed photographs of Ge/MMt

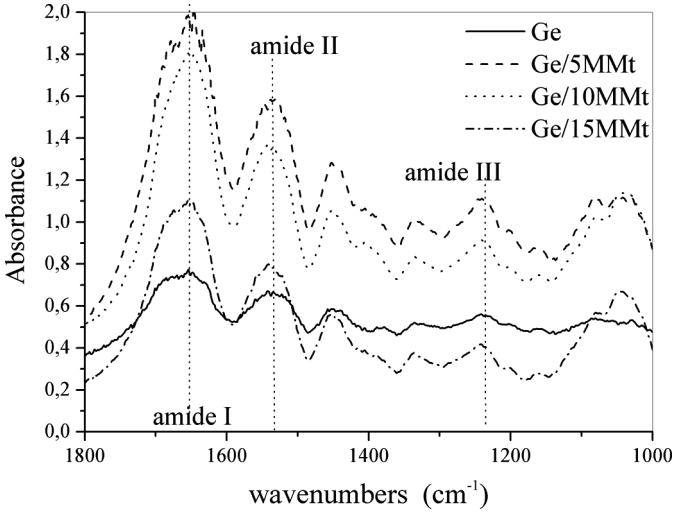

FIG. 2. FTIR spectra between 1800–1000 cm^{-1} for unfilled gelatin film, montmorillonite and Ge/MMt nanocomposites with 5 wt.%, 10 wt.% and 15 wt.% clay.

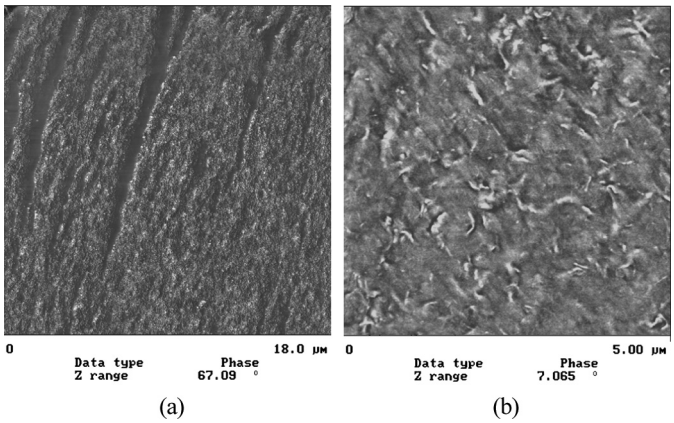

FIG. 3. HT-AFM phase images of (a) neat gelatin film and (b) Ge/10MMt nanocomposite film.

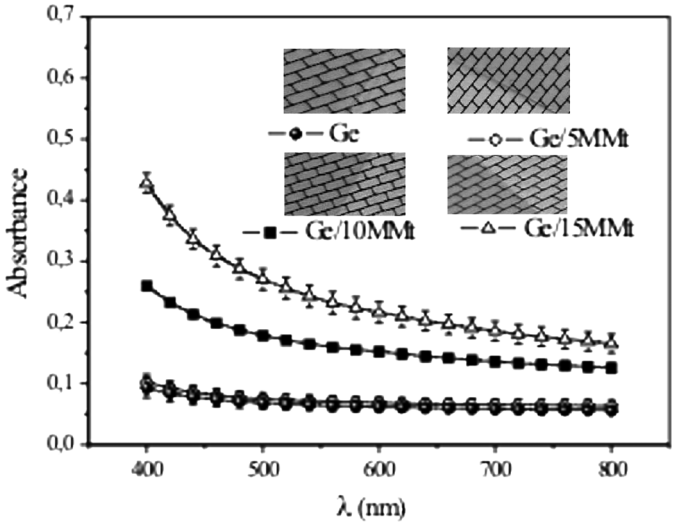

FIG. 4. Absorbance curves of unfilled gelatin and nanocomposites containing different amounts of MMt. Insets show photographs of the obtained films.

nanocomposite films with different clay contents. Compared to the unfilled-gelatin film, the composites were more opaque but all films remained transparent, regardless of MMt contents (within the MMt-content studied range). This was a desirable property in a material intended to be used in packaging applications.

Water uptake curves at 65% RH are represented in Figure 5. For all compositions the water absorption was rapid in the initial zone ($t < 200$ min). Beyond this time the absorption rate slowed down and leaded to a plateau corresponding to the water uptake at the equilibrium (WUeq). The WUeq values ranged between 21.3% and 20.6% (w/w) for the unfilled and nanocomposite filled with 15 wt.% clay, respectively. The slight improvement in water resistance was already reported for other nanocomposites based on biopolymers including thermoplastic starch[9,10,14], plasticized soy protein[11] and plasticized wheat protein[16].

In Ge/MMt bio-nanocomposites the reduction in water uptake probably accounted for by the combination of two effects: the water barrier property of the impermeable clay platelets making the pathway for water molecules to enter the Ge/MMt nanocomposite films more tortuous[5,12], and the occurrence of hydrogen bonding interactions between gelatin and clay, which increased surface hydrophobicity reducing the binding water capacity of the composites. This hypothesis was confirmed by calculating the dispersive and polar components as well as the surface energy as a function of clay content (Figure 6).

The addition of clay reduced the polar component and the surface energy of nanocomposite films, in agreement with a less hydrophilic surface. The water resistance of the nanocomposite films was quite increased by adding montmorillonite, in terms of both surface hydrophobicity and lower levels of water uptake. The addition of clay decreased D_{app} values form $21.8 \times 10^{-13}\,m^2/s$ to $5.1 \times 10^{-13}\,m^2/s$ for 15 wt.% clay (Table 1). Once again, this phenomenon evidenced that MMt provided a more tortuous path for permeant molecules and effectively lengthened the permeation route; therefore, water did not get through the nanocomposite film so easily in comparison with pure gelatin film.

The effect of clay content on WVP values measured at 65% RH is summarized in Table 1. Since water vapor

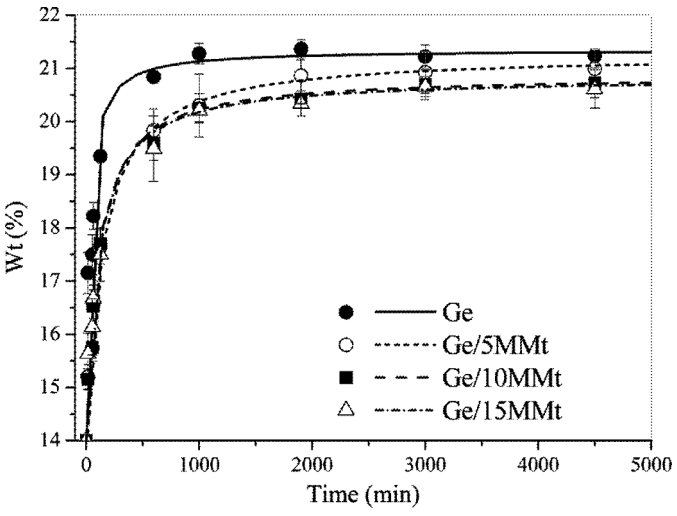

FIG. 5. Water absorption of unfilled gelatin film (●) and Ge/MMt nanocomposites with 5 wt.% (○), 10 wt.% (■) and 15 wt.% (Δ) clay.

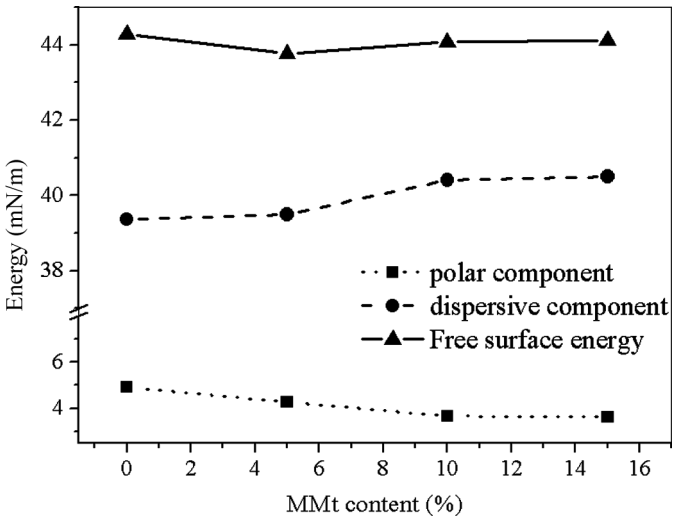

FIG. 6. Surface free energy, dispersive and polar components of nanocomposites as a function of clay loading.

TABLE 1
Apparent diffusion coefficient (Dapp) at 65%RH, water vapour permeability (WVP) at 65%RH, storage modulus (E*) and tan δ of Ge/MMt films

MMt content (wt.%)	$D_{app} \times 10^{13}$ (m^2/s)	$WVP \times 10^{14}$ (Kg.m/Pa.s.m^2)	E* (GPa)	tan δ (°C)
0	21.8 ± 5.6	17.3 ± 0.1	0.7 ± 0.1	104 ± 2
5	4.5 ± 0.8	16.0 ± 0.5	1.1 ± 0.2	114 ± 2
10	7.2 ± 1.5	7.1 ± 0.1	4.5 ± 0.3	123 ± 1
15	5.1 ± 1.1	5.1 ± 0.2	4.6 ± 0.2	126 ± 1

permeability of hydrophilic protein films is affected by film thickness, in the present study their variability was minimized and thicknesses were kept between 200–215 μm. The average WVP for the unfilled gelatin film was $17.3 \times 10^{-14}\,kg \cdot m/m^2 \cdot s \cdot Pa$, which was in the same range than that reported by Park et al.[34] for plasticized gelatin films obtained by casting. As expected from apparent diffusion coefficient estimations, WVP values decreased as clay loading increased (Table 1).

The water vapor barrier of Ge/MMt improved 3 times compared with that of control gelatin films. This was related to barrier role of silicate particles[5,6] and the establishment of strong hydrogen interactions between nanoclays and gelatin matrix. Similar results were found for other biopolymer/clay systems[12,14,16], but comparison between WVP values was rather difficult because of differences in film thickness and experimental conditions[35,36]. Depending on the clay content, Ge/MMt permeability values were comparable with those of enzymatic and chemically cross-linked plasticized-gelatin films ($1.2 \times 10^{-14}\,kg \cdot m/Pa \cdot s \cdot m^2$ and $1.5 \times 10^{-14}\,kg \cdot m/Pa \cdot s \cdot m^2$, respectively)[37], and that of poly(lactide) (PLA) ($4.66 \pm 0.25 \times 10^{-14}\,kg \cdot m/m^2 \cdot s \cdot Pa$, thickness: ca. 90 μm, prepared by solvent casting method)[36].

With regard to synthetic polymers, Ge/MMt films showed WVP values comparable to those of cellulose acetate (CA) ($0.5–1.6 \times 10^{-14}\,kg \cdot m/Pa \cdot s \cdot m^2$) but higher than those of high-density polyethylene (HPDE) ($2.4 \times 10^{-16}\,kg \cdot m/Pa \cdot s \cdot m^2$), poly(vinyl chloride) (PVC) ($0.7–2.4 \times 10^{-16}\,kg \cdot m/Pa \cdot s \cdot m^2$)[36] and low-density polyethylene (LDPE) ($3.6–9.7 \times 10^{-16}\,kg \cdot m/Pa \cdot s \cdot m^2$)[36,38].

The effect of MMt on the storage modulus (E′) and the tan delta (tan δ) peak of the Ge/MMt films as a function of the temperature is given in Figure 7. Values are reported in Table 1. As can be seen in Figure 7a, the storage modulus of Ge/10MMt and Ge/15MMt nanocomposite films improved compared to pure gelatin film, i.e., $E'_{Ge/10MMt} = 4.5$ GPa vs $E'_{Ge} = 0.7$ GPa. Particularly, composites with clay loading higher than 5 wt.% showed an improvement in E′ within the whole temperature range analyzed, which indicates that the addition of MMt extends the temperature application range of gelatin films.

On the other hand, *tan* δ peaks of the nanocomposites broadens and shift to higher temperatures by comparing to gelatin control films, indicating that MMt restrict

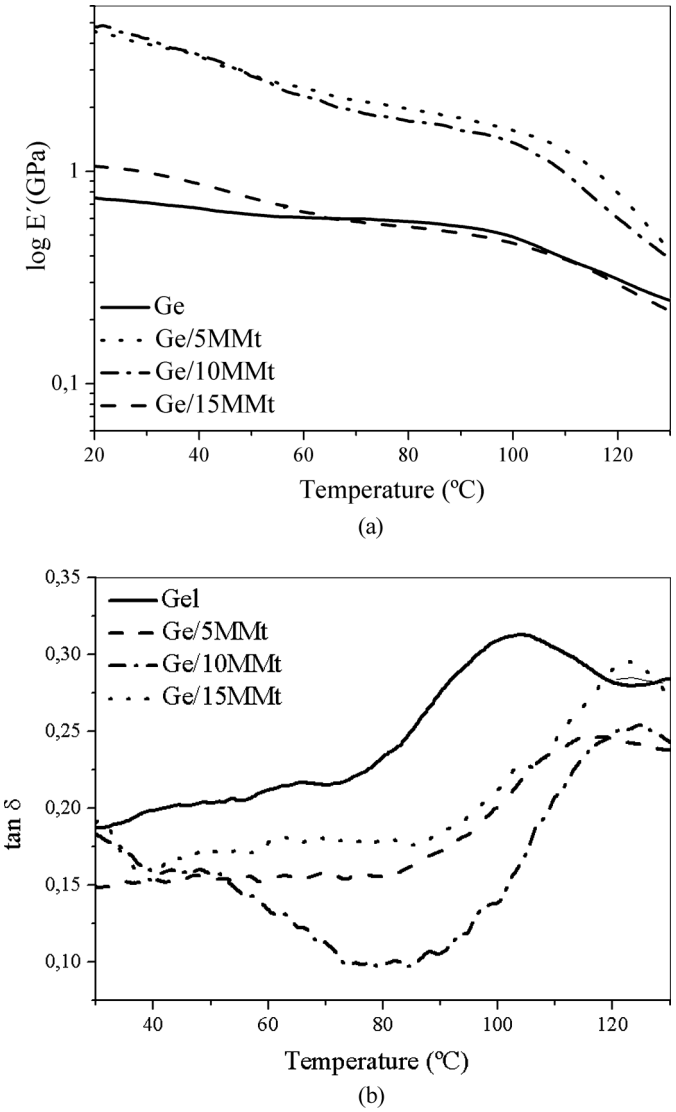

FIG. 7. (a) Storage modulus curves and (b) tan δ peaks from DMA of Ge/MMt and control films.

molecular motions in gelatin matrix, and acts as physical cross-linking points; during processing of the composites, the pre-existing hydrogen bonds between gelatin chains were replaced by new ones formed between gelatin and montmorillonite, as was evidenced by FTIR. The increment in storage modulus as well as the shift in *tan δ* peaks to higher temperatures for the nanocomposite evidenced a good interaction between the reinforcing phase and gelatin matrix.

CONCLUSIONS

Gelatin/montmorillonite nanocomposite films were successfully obtained for a variety of clay concentrations by casting technique assisted by ultrasonication without adding any compatibilizer or clay modifier. Ge/MMt nanocomposites kept the good optical transparency with MMt loading, indicating that filler was mostly distributed at the nanoscale. The obtained Ge/MMt films were more uniform in thickness and more water resistant than the unfilled counterpart. The presence of strong hydrogen interactions between gelatin and clay combined with the inherent barrier properties of the impermeable clay platelets resulted in the lowered surface hydrophilicity as well as WVP.

Besides water resistance, the storage modulii of nanocomposite films showed an increment in the temperature range analyzed and the tan δ peaks shifted to higher temperatures compared to pure gelatin film. Therefore, the addition of montmorillonite extends the temperature application range of gelatin films, improves moisture resistance and water vapor permeability without affecting transparency.

ACKNOWLEDGMENTS

Authors would like to express their gratitude to the National Research Council (CONICET, Argentina, PIP 6258/05) and to SECyT (APCyT, Argentina, PICT12-15074) for their financial support.

REFERENCES

1. Fraga, A.N.; Williams, R.J.J. Thermal properties of gelatin films. Polymer **1985**, *26*, 113–118.
2. Tharanathan, R.N. Films and composite coatings: Past, present and future. Trends Food Sci. Tech. **2003**, *14*, 71–78.
3. Huang, X.; Netravali, A. Characterization of nanoclay reinforced phitagel-modified soy protein concentrate resin. Biomacromolecules **2006**, *7*, 2783–2789.
4. Apostolov, A.A.; Fakirov, S.; Evstatiev, M.; Hoffmann, J.; Friedrich, K. Biodegradable laminates based on gelatin. 1. Preparation and mechanical properties. Macromol. Mater. Eng. **2002**, *287*, 693–697.
5. Alexandre, M.; Dubois, Ph. Polymer-layered silicate nanocomposite: Preparation, properties and uses of a new class of materials. Mater. Sci. Eng. **2001**, *28*, 1–63.
6. Ray, S.S.; Bousmina, M. Biodegradable polymers and their layered silicate nanocomposites: In greening the 21st century materials world. Prog. Polym. Sci. **2005**, *50*, 962–1079.
7. Zheng, J.P.; Li, P.; Ma, Y.L.; Yao, K.D. Gelatin/montmorillonite hybrid nanocomposite. 1. Preparation and properties. J. Appl. Polym. Sci. **2002**, *86*, 1189–1194.
8. Darder, M.; Colilla, M.; Ruiz-Hitzky, E. Biopolymer-clay nanocomposites based on chitosan intercalated in montmorillonite. Chem. Mater. **2003**, *15*, 3774–3780.
9. Huang, M.; Yu, J.; Ma, X.-F. Studies on the properties of montmorillonite-reinforced thermoplastic starch composites. Polymer **2004**, *45*, 7017–7023.
10. Chen, B.; Evans, J.R.G. Thermoplastic starch-clay nanocomposites and their characteristics. Carbohyd. Polym. **2005**, *61*, 455–463.
11. Chen, P.; Zhang, L. Interaction and properties of highly exfoliated soy protein/montmorillonite nanocomposites. Biomacromolecules **2006**, *7*, 1700–1706.
12. Hedenqvist, M.S.; Backman, A.; Gallstedt, M.; Boyd, R.H.; Gedde, U.W. Morphology and diffusion properties of whey/montmorillonite nanocomposites. Compos. Sci. Technol. **2006**, *66*, 2350–2359.
13. Günister, E.; Pestreli, D.; Ünlü, C.H.; Atici, O.; Güngör, N. Synthesis and characterization of Chitosan-MMT biocomposite systems. Carbohyd. Polym. **2007**, *67*, 358–365.
14. Kampeerapappun, P.; Aht-ong, D.; Pentrakoon, D.; Srikulkit, K. Preparation of cassava starch/montmorillonite composite films. Carbohyd. Polym. **2007**, *67*, 155–163.
15. Martucci, J.F.; Vazquez, A.; Ruseckaite, R.A. Nanocomposite based on gelatin and montmorillonite. Morphological and thermal studies. J. Therm. Anal. Calorim. **2007**, *89*, 117–122.
16. Tunc, S.; Angellier, H.; Cahyana, Y.; Chalier, P.; Gontard, N.; Gastaldi, E. Functional properties of wheat gluten/montmorillonite nanocomposite films processed by casting. J. Membr. Sci. **2007**, *289*, 159–168.
17. Sorrentino, A.; Gorrasi, G.; Vittoria, V. Potential perspectives of bio-nanocomposites for food packaging applications. Trends Food Sci. Tech. **2007**, *18*, 84–95.
18. Koo, C.M.; Ham, H.T.; Choi, M.H.; Kim, S.O.; Cheng, I.J. Characteristics of polyvinylpyrrolidone-layered silicate nanocomposites prepared by attrition ball milling. Polymer **2003**, *44*, 681–689.
19. Pandey, J.K.; Raghunatha Reddy, K.; Pratheep Kumar, A.; Singh, R.P. An overview on the degradability of polymer nanocomposites. Polym. Degrad. Stabil. **2005**, *88*, 234–250.
20. Martucci, J.F.; Ruseckaite, R.A. Biodegradation of three-layer laminate films based on gelatin under indoor soil conditions. Polym. Degrad. Stabil. **2009**, *94*, 1307–1313.
21. Southern Clay Products Cloisite Na^+, Nanoclay Technical Report, www.scprod.com
22. Xu, S.W.; Zheng, J.P.; Tong, L.; De Yao, K. Interactions of functional groups of gelatin and montmorillonite in nancomposite. J. Appl. Polym. Sci. **2006**, *101*, 1556–1561.
23. Irissin-Mangata, J.; Bauduin, G.; Boutevin, B.; Gontard, N. New plasticizers for wheat gluten films. Eur. Polym. J. **2001**, *37*, 1533–1541.
24. Shimizu, R.H.; Demarquette, N.R. Evaluation of surface energy of solid polymers using different models. J. Appl. Polym. Sci. **2000**, *76*, 1931–1845.
25. Dufresne, A.; Kellerhals, M.B.; Witholt, B. Transcrystallization in Mcl-PHAs/cellulose whiskers composite. Macromolecules **1999**, *32*, 7396–7401.
26. Anglès, M.N.; Dufresne, A. Plasticized starch/tunicin whiskers nanocomposites. 1. Structural analysis. Macromolecules **2000**, *33*, 8344–8353.
27. Merdas, I.; Thominette, F.; Tcharkhtchi, A.; Verdu, J. Factors governing water absorption by composite matrices. Compos. Sci. Technol. **2002**, *62*, 487–492.
28. Grevellec, J.I.; Marquie, C.; Ferry, L.; Crespy, A.; Vialettes, V. Processability of cottonseed proteins into biodegradable materials. Biomacromolecules **2001**, *2*, 1104–1109.

29. Zhang, X.; Xu, R.; Wu, Z.; Zhou, C. The synthesis and characterization of polyurethane/clay nanocomposites. Polym. Int. **2003**, *52*, 790–794.
30. Viville, P.; Lazzaroni, R.; Mollet, E.; Alexandre, M.; Dubois, Ph.; Borcia, G.; Pireaux, J.-J. Surface characterization of poly(e-caprolactone)-based nanocomposites. Langmuir **2003**, *19*, 9425–9433.
31. Sionkowska, A.; Wisniewski, M.; Skopinska, J.; Kennedy, C.J.; Wess, T.J. Molecular interactions in collagen and chitosan blends. Biomaterials **2004**, *25*, 795–801.
32. Kiersnowski, A.; Pigłowski, J. Polymer-layered silicate nanocomposites based on poly(e-caprolactone). Eur. Polym. J. **2004**, *40*, 1199–1207.
33. Yalcin, B.; Cakmak, M. The role of plasticizer on the exfoliation and dispersion and fracture behavior of clay particles in PVC matrix: A comprehensive morphological study. Polymer **2004**, *45*, 6623–6638.
34. Park, J.W.; Scott Whiteside, W.; Cho, S.Y. Mechanical and water vapor barrier properties of extruded and heat-pressed gelatin films. LWT Food Sci. Technol. **2008**, *41*, 692–700.
35. Gennadios, A.; Weller, C.L.; Gooding, C.H. Measurements errors in water vapor permeability of highly permeable, hydrophilic edible films. J. Food Eng. **1994**, *21*, 395–409.
36. Rhim, J.-W.; Mohanty, K.A.; Singh, S.P.; Ng, P.K.W. Preparation and properties of biodegradable multilayer films based on soy protein isolate and poly(lactide). Ind. Eng. Chem. Res. **2006**, *45*, 3059–3066.
37. de Carvalho, R.A.; Ferreira Grosso, C.R. Characterization of gelatin based films modified with transglutaminase, glyoxal and formaldehyde. Food Hydrocoll. **2004**, *18*, 717–726.
38. Shellhammer, T.H.; Krochta, J.M. Whey protein emulsion film performance as affected by lipid type and amount. J. Food Sci. **1997**, *62*, 390–394.